Global-Scale Intraseasonal Oscillations of Outgoing Longwave Radiation and 250 mb Zonal Wind during Northern Hemisphere Summer

THOMAS R. KNUTSON,* KLAUS M. WEICKMANN AND JOHN E. KUTZBACH

Center for Climatic Research, University of Wisconsin—Madison, Madison, WI 53706

(Manuscript received 13 March 1985, in final form 7 October 1985)

ABSTRACT

Intraseasonal fluctuations of satellite-based observations of outgoing longwave radiation (OLR) and NMC analyses of 250 mb zonal wind (U250) are described based on global data from nine Northern Hemisphere summers (May–October). Cross-spectral analysis of the 28–72 day spectral band is used to establish statistically significant relationships for the entire data period. Hovmöller diagrams are used to examine individual events and to estimate the oscillation's time scale and propagation characteristics.

Intraseasonal OLR fluctuations have their greatest amplitude in the Indian monsoon region and north of the equator in the western tropical Pacific. These two regions have out-of-phase fluctuations and appear to be linked by OLR anomalies propagating eastward (at 3–6 m s^{-1}) along the equator between 50° and 160°E. The OLR oscillation has a preferred time scale of 30–60 days during May–October, based on a sample of more than 30 events. The initiation near the equator of northward-propagating (1–2 m s^{-1}) OLR anomalies in the Indian monsoon region is also associated with the eastward-propagating equatorial OLR anomalies.

The U250 intraseasonal fluctuations have a prominent zonal wavenumber-one structure throughout the tropics with the exception of the Northern Hemisphere tropics over the Atlantic, Africa, and the Indian monsoon region. The U250 anomalies propagate eastward along 0°–10°S at about 6 m s^{-1} from 40° to 160°E and at about 15 m s^{-1} from 160°E to 0°W. These longitudinal changes in the oscillation's ground speed may be due in part to longitudinal changes in the zonal wind basic state. The 28–72 day U250 anomalies along 30°S (50°S) are out of phase (in phase) with the tropical U250 anomalies over most of the Pacific and Indian Ocean sectors.

The phase relationships between tropical OLR and U250 anomalies seem dynamically consistent, generally showing 250 mb *u*-component divergence flanking regions of convection. Although the eastward propagation of OLR anomalies along 5°N–5°S is not continuous around the globe, areas of significant coherence scattered throughout the tropics exhibit a zonal wavenumber-one phase structure. In these remote regions, OLR anomalies may be dynamically linked by an eastward-propagating tropical circulation feature.

1. Introduction

Following the early work of Madden and Julian (1971, 1972) observational studies in the last decade have shown that large-scale quasi-periodic oscillations with time scales of a few weeks to a few months occur in many parts of the world, particularly within the tropics. This report focuses on statistically significant observational evidence for these oscillations in nine-year data sets of outgoing longwave radiation (OLR) and 250 mb zonal wind (U250). The season analyzed here covers the 180-day period from 1 May to 27 October, hereafter referred to as Northern Hemisphere (NH) summer, although it also corresponds to the Southern Hemisphere winter season. The term "tropics" used here will refer to the region of the globe lying roughly between 20°N and 20°S.

2. Review of previous work

Madden and Julian (1971, 1972) presented evidence for a statistically significant zonal wind oscillation in the tropics and described some of the features of the oscillation, which they noted had a quasi-periodic nature with a time scale of 40–50 days. They described the phenomenon as a global-scale zonally oriented circulation cell that propagated eastward and was situated in the tropics. They noted that the oscillation primarily involved the zonal wind with the upper and lower tropospheric wind anomalies being out of phase with each other.

In another early paper, Parker (1973) found quasi-periodic zonal wind oscillations primarily confined to the 70–150 mb region, with a time scale of 25–40 days. He concluded that the oscillations were equatorial Kelvin waves, with zonal wavenumber-one horizontal structure, propagating eastward around the globe.

Yasunari (1980, 1981) found evidence for 40-day fluctuations in the Indian monsoon region convective

* Present Affiliation: Geophysical Fluid Dynamics Laboratory/NOAA, Princeton, NJ.

activity during Northern Hemisphere summer. The anomalies generally propagated northward from the equator to the northern extent of the monsoon region. He concluded that the oscillations were related to the active-break cycles in the Indian monsoon. Julian and Madden (1981) presented further evidence for the role of convection in the oscillation and agreed with Yasunari's conclusion that the northward-propagating monsoon oscillations were part of the same phenomenon as their eastward-propagating tropical oscillations.

Recently, a number of studies have documented further evidence for these intraseasonal oscillations. Sikka and Gadgil (1980), Krishnamurti and Subrahmanyam (1982) and T. Murakami et al. (1983) have examined oscillations in convection and circulation in the Indian monsoon region during Northern Hemisphere summer, while Maruyama (1982), Takeda and Ikeyama (1984), Quah (1984) and M. Murakami (1984) have reported on the occurrence of oscillations in the western Pacific.

Global-scale aspects of the oscillation have been studied by Lau and Chan (1983a,b), who used monthly average OLR data and by Lorenc (1984) and Krishnamurti et al. (1985) who studied global velocity potential fields for 1979. Weickmann (1983) noted an apparent relationship between large-scale eastward-propagating tropical OLR anomalies and large-scale extratropical circulation modes, using NMC vector wind data (850 and 250 mb) for six Northern Hemisphere winters.

Statistically significant evidence for these oscillations and the links between the upper air circulation and convection anomalies was presented by Weickmann, Lussky and Kutzbach (1985, hereafter referred to as WLK) based upon cross-spectral analyses of 28–72 day oscillations of OLR and 250 mb streamfunction during 10 NH winter seasons. A typical life cycle of the oscillation was presented showing the spatial and temporal details of these relationships.

This paper will examine the statistical evidence for intraseasonal oscillations in OLR and U250 during nine NH summers. Cross-spectral analysis of five-day averaged data is used to show what significant phase relationships are present for the individual variables as well as between the OLR and U250 data fields. Hovmöller diagrams will be used to examine the climatology of the oscillations and to illustrate propagation and other features of individual events.

Because the data set examined here for intraseasonal oscillations is longer than in most previous studies, with more than 30 occurrences of the oscillation identified in the nine NH summers, the results from this study will emphasize the characteristics of the oscillation that have occurred frequently in a reasonably large sample. Our results will show that a fair amount of variability occurs in the behavior of the intraseasonal oscillations, which means that one should exercise caution when drawing conclusions based upon a small sample of the events.

Some earlier studies of the oscillation (e.g., Madden and Julian, 1971, 1972) have dealt with full-year data sets. However, large seasonal changes take place in the basic state in which the oscillations occur—for example, locations of primary convection regions, jet streams, persistent high pressure regions, and areas of large land–sea temperature contrasts. This suggests that a separate examination of two distinct seasons can help identify how changes in these parameters affect the oscillations. A detailed *comparison* between the oscillation during the NH summer and NH winter seasons is the subject of a forthcoming paper.

Our upper-air wind analysis differs from that of Madden and Julian in that their results were based upon a relatively small number of tropical rawindsonde stations while our coverage is global and stems from the NMC analysis scheme. In addition, Madden and Julian's (1972) rawindsonde data consisted of up to 10 years of record from the years 1957–67 while our data record is from 1974 to 1983. Thus the two studies can help us learn about the oscillation's behavior during two separate time periods.

While this paper emphasizes observed rather than theoretical or modeled aspects of the oscillation, several preliminary theoretical and modeling studies have been published. A review and discussion of theoretical aspects of the oscillation is presented in the discussion section.

3. Data description

The OLR data set consists of nine Northern Hemisphere summers (1974–83, with 1978 missing) of non-overlapping five-day averages or pentads. The OLR data are derived from twice-daily (12-hour interval) measurements taken from NOAA polar-orbiting satellites, and are described more fully in Gruber and Winston (1978). The data have a horizontal resolution of 5° × 5° from 85°N to 85°S and were obtained by extracting one-fourth of the values from the original 2.5° × 2.5° grids. The first six pentads of NH summer 1974 were missing. The data for one isolated missing pentad (23–27 September 1983) were estimated by linear interpolation.

In tropical latitudes where surface temperature contrasts are relatively small in most areas, low OLR values correspond to regions of high cloudiness associated with deep convection. In higher latitudes, the interpretation is less clear, with low surface temperatures also producing low OLR readings. This paper emphasizes OLR fluctuations in lower latitudes and will use the terms negative OLR anomaly and positive convection or cloudiness anomaly interchangeably.

The mean OLR map for nine NH summers (Fig. 1a) shows relatively high OLR values in the regions of the subtropical highs as well as over large desert regions. These areas are characterized by relatively rare occurrences of convective activity. In the tropics, relatively cloudy regions are centered north of the equator in

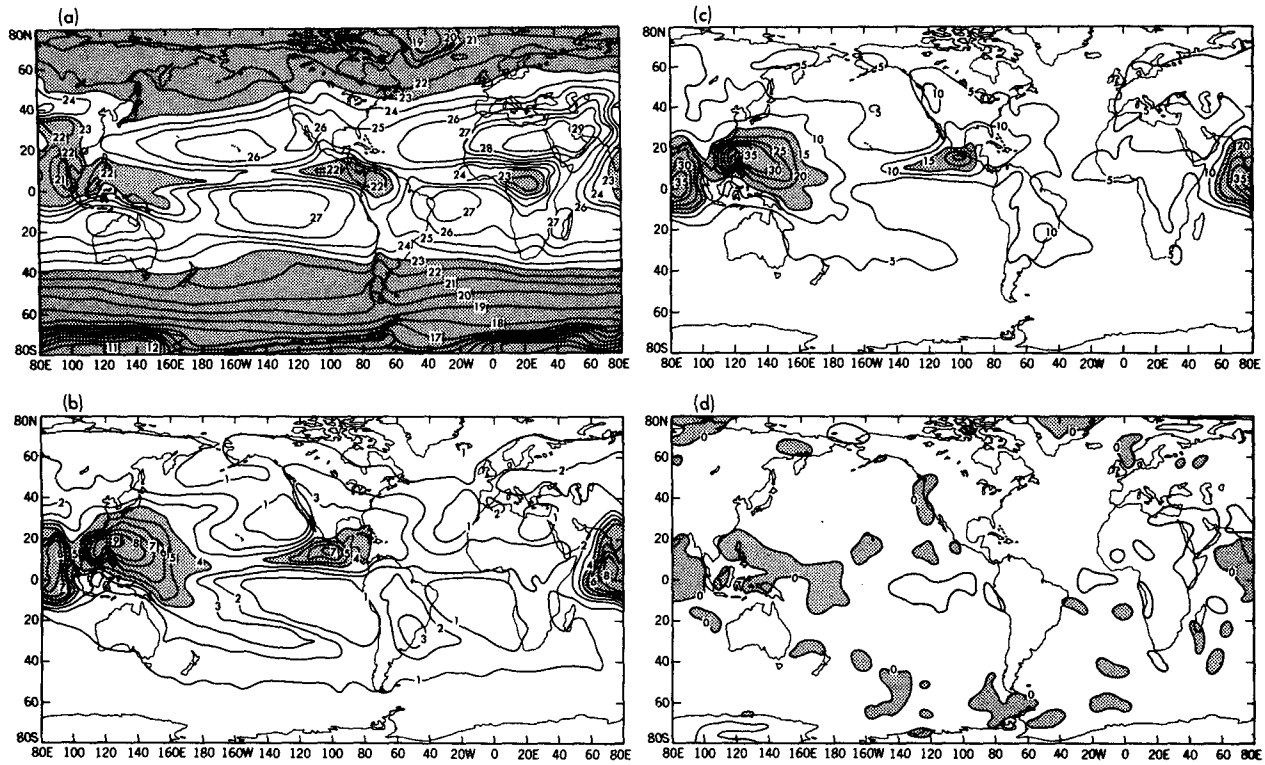

FIG. 1. May–October outgoing longwave radiation (OLR) statistics, based on nine NH summers (1974–83, with 1978 missing): (a) NH summer mean with shaded areas representing regions with values less than 230 W m^{-2}. Contour interval of 20 W m^{-2}; contour labels are divided by 10. (b) Ensemble intraseasonal variance with shaded regions indicating values greater than 400 (W m^{-2})^2. Contour interval is 100 (W m^{-2})^2; contour labels are divided by 100. (c) Ensemble 28–72 day variance with shaded regions indicating values greater than 150 (W m^{-2})^2. Contour interval is 50 (W m^{-2})^2; contour labels are divided by 10. (d) Shaded regions indicate where OLR ensemble 28–72 day variance exceeds a red noise background variance at the 95% significance level.

Africa, Central and South America and Southern Asia, which are areas of frequent convective activity. The low OLR values at higher latitudes are caused in large part by lower surface temperatures.

The upper air circulation data consist of nine NH summer seasons (1975–83) of 250 mb zonal wind pentads. These data were derived from twice-daily NMC global analyses and have a horizontal resolution of 5° × 5°. Eight isolated or paired missing pentads were estimated by linear interpolation. From 45° to 85°S, data are only available since 30 June 1976. The degrees of freedom used in the significance tests were adjusted for the missing or interpolated data. The NMC analysis scheme was changed on 22 September 1978 from Flattery's (1971) analysis, where the fields were expressed using Hough functions, to optimum interpolation (Bergman, 1979; McPherson et al., 1979).

We use the 250 mb u-component of the wind in our analysis since the studies of Madden and Julian (1971, 1972), Maruyama (1982), and others have shown that the tropical oscillation involves primarily the zonal wind. The advantage of the zonal wind over 250 mb streamfunction (e.g., WLK) is that information on the zonal component of the divergent wind field is retained. The disadvantage is that the meridional wind is left out of the analysis. One might expect the divergence of the zonal wind to be large in association with the tropical convection, although the meridional wind may also play an important part in the oscillation, particularly in the case of related extratropical circulation features.

The nine-season mean 250 mb vector wind field is shown in Fig. 2a. The strongest U250 winds occur in the Southern Hemisphere over and to the east of Australia along 30°S. To the east of this jet core is a midlatitude jet stream generally located in the 40°–50°S latitude band. There is a weak tropical easterly jet in the Northern Hemisphere monsoon region; the weakness of this feature may be at least partially explained by the fact that Fig. 2a presents mean conditions for the six-month period May–October rather than conditions occurring at the height of the monsoon. In the Northern Hemisphere the subtropical and midlatitude westerly jet streams are much weaker than they are in the NH winter season.

4. Methods of analysis

The primary focus of this study is variability of the atmosphere on time scales of one to two months. The averaging of 10 twice-daily wind analyses to form a pentad reduces the aliasing effects of fluctuations with time scales of less than 10 days.

The annual and semiannual cycles are prominent features in both data sets. They were removed by subtracting the first two Fourier harmonics of the mean seasonal cycle (for the full-year data set) from each individual year. The annual and semiannual cycles of data sets nearly identical to the ones used here are described in Kutzbach and Weickmann (1984).

The interannual variability of the OLR and U250 data was removed by subtracting the mean of each individual season prior to its analysis. The linear trend for each individual season was removed prior to the Fourier analysis. No tapering was done to any of the time series. The final input to the Fourier analysis routines was nine 36-pentad anomaly series for each of the 2520 points of the global grid.

Of the 18 Fourier frequencies available (1, 2, . . . , 18 cycles per 180 days), we have chosen to emphasize the four frequencies containing variance on time scales of 28–72 days (Fourier frequencies of 3–6 cycles per 180 days, with half-bandwidths extending from 2.5–6.5 cycles per 180 days.) Our analysis of the oscillation's periodicity, which will be presented later in this report, will show that the 28–72 day band is an appropriate one for studying the oscillation.

For the spectral and cross spectral analyses, the variance at these frequencies was summed for individual seasons after which the 28–72 day variance was averaged over the nine seasons to obtain an ensemble summer spectrum. The degrees of freedom associated with each season's four frequencies were also summed. For the purpose of assessing the statistical significance of the results, the ensemble 28–72 day variance was compared to a red noise background variance which was based upon the lag-one autocorrelation coefficient (Gilman et al., 1963). This may not be the optimum background spectrum to use for comparison, but it does take into account some of the effects of persistence in the data.

The phase and coherence-squared values in the cross-spectral analysis (see for example Rayner, 1971) were based upon eight-season ensemble averages of the four frequencies mentioned above, with 1974 and 1978 not included because of missing OLR or U250 data. The significance of the coherence-squared statistic was assessed following Julian (1975), while the significance of the variance spectra was established based upon the chi-square over degrees of freedom distribution. Further discussion of the methods of analysis is given in WLK.

5. Results of spectral analysis

a. Outgoing longwave radiation

Summing the variance in all 18 frequencies of the nine-season ensemble spectrum, one obtains the ensemble intraseasonal (10–180 day) variance map for the anomaly series (Fig. 1b). The variance in the 28–72 day band of the spectrum (4 out of 18 frequencies) is shown in Fig. 1c. The areas of most prominent 10–180 day variance and 28–72 day variance generally coincide. The largest 28–72 day variance for the NH summer season is found primarily north of the equator in three regions: 1) the eastern tropical Pacific west of Central America; 2) the western tropical Pacific from Southeast Asia to the dateline; and 3) the Indian monsoon region, extending from about 20°N to 10°S. The regions of large variability in the western tropical Pacific and Indian monsoon region are separated by a local minimum in variability near 100°E.

Comparison of Fig. 1b, c with the summer mean OLR map (Fig. 1a) reveals that the three areas of large variability are located in areas of frequent deep convection. However, over certain other regions of frequent convection, large variability is not apparent on either the maps of total intraseasonal variance or 28–72 day variance. This is particularly striking over two major tropical land regions—equatorial Africa and northern South America. Thus, it appears that the largest intraseasonal and 28–72 day OLR variability tends to occur over those tropical *oceanic* regions which are favorable for convection, as opposed to tropical land masses.

Within the tropics, the regions of lowest OLR variability are in the South Atlantic and eastern South Pacific. Figure 1a shows that these regions have high NH summer-mean OLR values. These regions of infrequent deep convection are influenced by strong subtropical highs as well as relatively low sea surface temperatures.

In order to determine regions of statistically significant 28–72 day OLR variability, the ensemble variance and the ensemble red-noise background variance for the 28–72 day band were compared. The shaded regions in Fig. 1d indicate areas where the 28–72 day variance exceeds the red-noise background variance at the 95% significance level. About 16% of the global area is significant above red noise at the 95% level. For this calculation, the number of grid points exceeding the 95% level at each latitude was weighted by the cosine of latitude to achieve equal-area weighting on the sphere.

The major areas of significance are in the tropical western Pacific and the Indian monsoon region. These areas tend to be centered north of the equator in the tropical band. Outside the tropics, some areas of significance occur, but they are not emphasized in this report.

b. 250 mb zonal wind

Similar maps to those discussed above were constructed for the 250 mb zonal wind (U250). The maps of ensemble intraseasonal (10–180 day) variance (Fig. 2b) and ensemble 28–72 day variance (Fig. 2c) show that the largest variations of U250 occur outside the

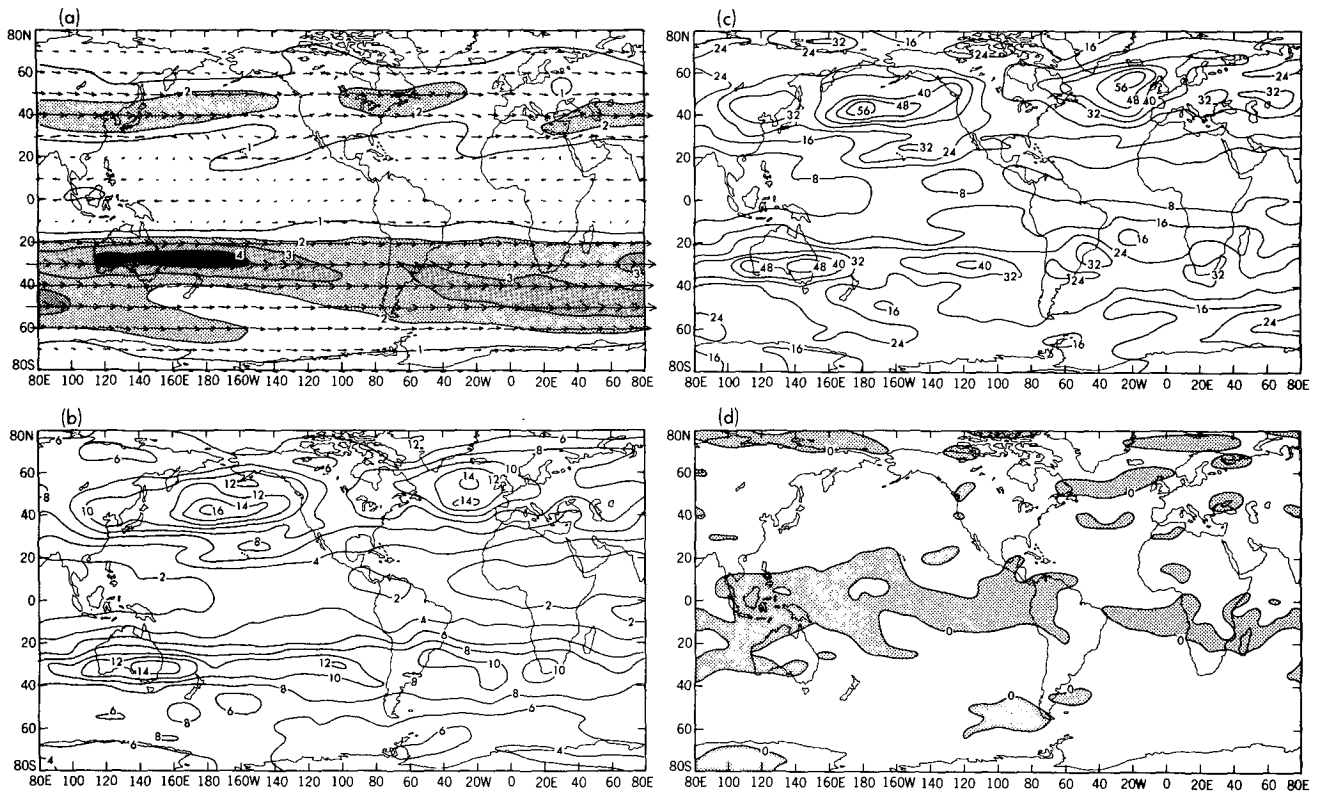

FIG. 2. May–October 250 mb wind field statistics, based on nine seasons (1975–83): (a) NH summer mean 250 mb vector wind field. Contour interval is 10 m s^{-1}; contour labels are divided by 10. Shaded regions represent velocity magnitudes as follows: light shading—20–30 m s^{-1}; medium shading—30–40 m s^{-1}; dark shading—40–50 m s^{-1}. (b) 250 mb zonal wind (U250) ensemble intraseasonal variance. Contour interval is 20 (m s^{-1})^2; contour labels are divided by 10. (c) U250 ensemble 28–72 day variance. Contour interval is 8 (m s^{-1})^2. (d) Shaded regions indicate where U250 ensemble 28–72 day variance is significantly above a red-noise background variance at the 95% level.

tropics in the regions of the climatological mean jet streams in both hemispheres (Fig. 2a).

However, Fig. 2d shows that the major regions of significant 28–72 day fluctuations, compared to a red-noise background, are found in the tropics, separate from the regions of maximum variability. Some smaller zonally oriented bands of significant 28–72 day variations occur in the Northern Hemisphere, particularly over the Atlantic. About 25% of the globe has fluctuations above red noise at the 95% significance level, which represents a very large signal in terms of spatial coverage.

During NH summer the major tropical areas of significant U250 fluctuations lie somewhat to the east of the major tropical areas of significant OLR fluctuations. Many of the regions of significance for U250 are found in areas of relatively poor data coverage by radiosondes; therefore, these regions have potentially large errors in the NMC analysis (McPherson et al., 1979).

In summary, based on Fig. 2, we conclude that while the NH summer intraseasonal variability of U250 in the tropics is small compared to that of middle latitude locations, the oscillations that do occur are strongly associated with the 28–72 day time scale over an extensive area of the tropics.

6. Cross-spectral analysis (OLR vs OLR)

By performing cross-spectral analyses between a reference OLR time series and all other OLR time series on a global grid, the propagation features and spatial phase relationships of the 28–72 day OLR oscillations can be explored. The reference time series consisted of an equal-weight average of the time series of a center point and its four neighboring points. A total of 35 global analyses were performed, of which four are displayed in Fig. 3 for the latitudinal domain 40°N to 40°S.

The length of each small arrow indicates how statistically significant the coherence relationship is between a grid point and the reference series (see caption). In map A, about 11% of the globe has a coherence-squared value that is significant at the 99% level. In all the maps there is a tendency for a fairly large number of points near the center point to have high coherence-squared values.

The direction of the small arrows corresponds to a time series' phase relative to the reference series. For example, in map A the phase arrows near 0°, 80°E point to a "nine o'clock" position, indicating that 28–72 day oscillations in that region tend to lead those at

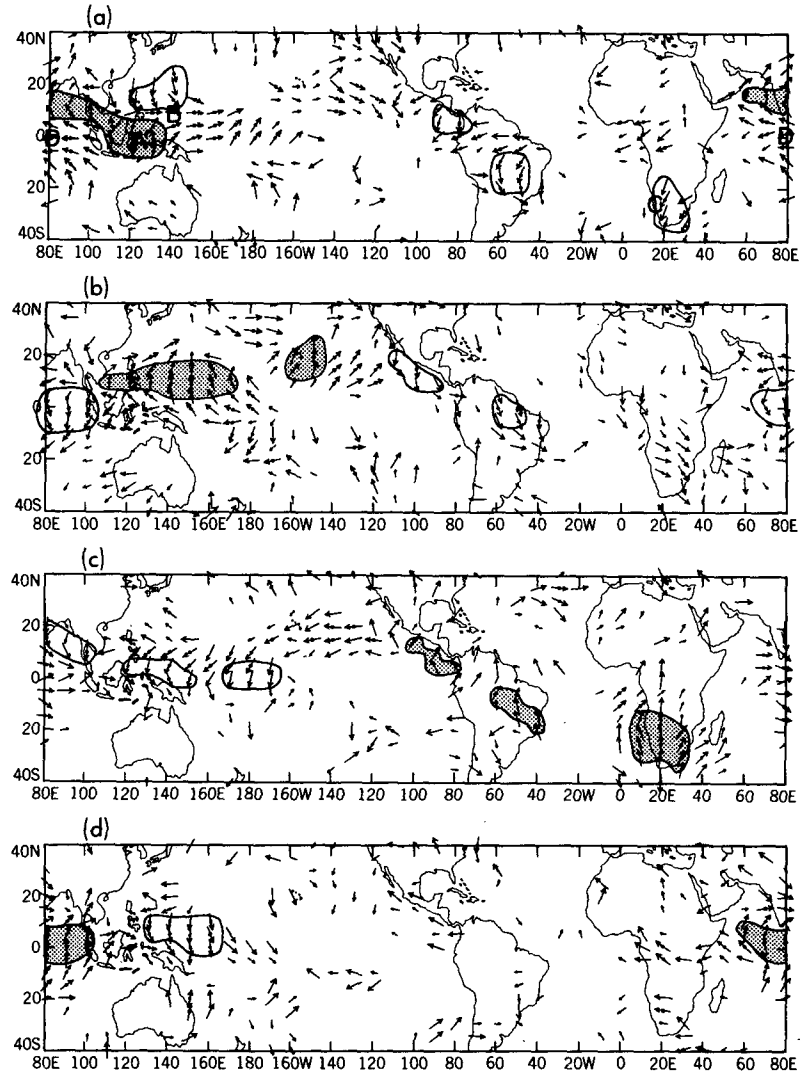

FIG. 3. Phase and coherence-squared information for a 28–72 day cross-spectral analysis between OLR and OLR, using five grid-point regions centered at (a) 0°, 120°E; (b) 10°N, 140°E; (c) 25°S, 20°E; and (d) 0°, 80°E as the reference series. The *lengths* of the small arrows are proportional to *coherence-squared;* arrows are plotted only where the coherence-squared exceeds the 80% significance level. Locations where the coherence-squared exceeds the 99% level have arrows of uniform length with a small box on the shaft. Information is plotted for every other longitude available. The *directions* of the small arrows indicate the *phase* of 28–72 day variations relative to the base point. (See text.) Shaded (unshaded) outlined regions on each map indicate where cloudiness (clear) anomalies occur at ¼ cycle intervals during a "typical" 28–72 day oscillation.

0°, 120°E by about ¼ cycle (or about 10 days). Arrows pointing in opposite directions indicate time series that are about 180° out of phase.

On map A, the superimposed letters B, C, and D identify locations where OLR fluctuations lag those at 0°, 120°E by about ¼, ½, and ¾ cycle, respectively. Cross spectral results for OLR time series centered at these locations are displayed in Fig. 3 (B–D). These particular analyses were selected from a larger set of maps for display because the phase relationships between key regions were most consistent for these locations.

The sequence of maps illustrates the spatial and temporal evolution of cloudiness anomalies during an oscillation. The outlined regions are subjective analyses, based on results from several maps, indicating areas with coherent 28–72 day fluctuations that are roughly in-phase or out-of-phase with the reference series. Thus the shaded (unshaded) outlined regions can be interpreted as representing the locations of cloudiness (clear) anomalies at ¼ cycle intervals (about 10 days) during a "typical" oscillation, based on all the 28–72 day oscillations in the nine NH summers of record.

The map sequence arbitrarily starts with map A in

which convection anomalies are located along the equator in central Indonesia and over southern India. Anomalously clear conditions are found in the western tropical Pacific, southern Africa and South America. About 10 days later (map B) the convection has moved eastward and north of the equator in the western Pacific, while there is some evidence for cloudiness anomalies near Hawaii. Anomalously clear conditions are now found in the equatorial Indian Ocean.

Map C shows cloudiness anomalies occurring simultaneously in three separate regions (extreme eastern tropical Pacific, eastern tropical South America, and southern Africa). Additional evidence for coherent in-phase fluctuations in these three regions is found in maps A and B. The southern Africa region appears more prominent than the other regions in map C because the reference series is located there. At this point in the oscillation, anomalously clear conditions have progressed to the northern part of the Indian monsoon region and to the western tropical Pacific. Maps A and C both illustrate the zonal wavenumber-one structure of the oscillation, with convective activity in the Indian monsoon region and western tropical Pacific being approximately out-of-phase with convection anomalies in southern Africa and South America. In about 10 days, the cloudiness returns to the equatorial Indian Ocean (map D), from where it progresses northward to India and eastward to Indonesia (map A) to complete the cycle.

A comparison of the phase and coherence relationships on the four maps shows that the most consistent relationships are found in the Indian monsoon region and western Pacific, which is where the largest 28–72 day variability is located (Fig. 1c). The direction of phase propagation of anomalies on individual maps is determined by following a sequence of phase arrows that "rotate clockwise" from one arrow to the next. In all the maps there is evidence for northward propagation of OLR anomalies in the Indian monsoon region along 70° and 80°E from the equator to around 25°N, which is in agreement with the results of Yasunari (1980), Sikka and Gadgil (1980) and others. Northward propagation also occurs in the western tropical Pacific along 120°–140°E from the equator to 20°N. There is evidence for prominent eastward propagation of OLR anomalies along the equator from 60° to 160°E. The northward-moving and eastward-moving OLR anomalies are phase-locked since they occur simultaneously near the equator.

While the OLR anomalies have some characteristics of an eastward-propagating wavenumber-one structure in the tropics, consistent gaps in the wavenumber-one structure occur in areas of relatively high mean OLR values (Fig. 1a)—particularly the eastern tropical Pacific and the tropical south Atlantic. Regions of relatively frequent convection in the Northern Hemisphere over tropical Africa and the tropical Atlantic do not appear to be strongly affected by the oscillation. Nevertheless, while Fig. 1c indicates that 28–72 day OLR fluctuations have their greatest magnitude in the Indian monsoon region and western tropical Pacific, the organized global-scale structure we have described may be an important element of the oscillation.

7. Outgoing longwave radiation Hovmöller diagram analyses

In order to supplement the statistical results obtained from the cross spectral analysis, OLR anomalies are displayed in longitude vs time format in Fig. 4. While the phase/coherence maps (Fig. 3) show average or composite features of the OLR oscillation, the Hovmöller diagrams reveal some of the characteristics of individual events as well as some important differences between events. The extra features drawn on the diagrams for 1979 and 1981 will be discussed in section 10.

The seasonal means (interannual variability) and the annual and semiannual cycles of OLR were removed for each grid point in the same manner as for the spectral analysis. However, for the Hovmöller diagrams, the linear trend for each season was not removed. Thus, these diagrams contain seasonal trends plus variability with time scales of 10 days to a full season, in contrast to the 28–72 day time scale of the cross-spectral analysis. OLR values were averaged from 5°N to 5°S since our cross-spectral results (Fig. 3) showed prominent eastward propagation in this latitudinal band from 50° to 160°E as well as coherent anomalies near 80°W and 10°E.

While there is evidence for the eastward propagation in all years, there is considerable variability among the seasons in the amplitude, periodicity, propagation speed, and general prominence of the intraseasonal events. Prominent oscillations occurred in the NH summers of 1980, 1981, 1983, and May–June 1982. Some of the OLR oscillations in the diagrams exhibit characteristics of a dipole phenomenon (e.g., May–July 1976) with the centers of maximum variability remaining stationary along the equator at about 80° and 150°E and no prominent propagation of anomalies between the two centers. However, in the majority of cases, there is clear evidence for an eastward propagating anomaly between these two regions. This supports an interpretation of the OLR oscillation as an eastward propagating feature (with the Indian Ocean and western tropical Pacific regions having an amplified out-of-phase response) as opposed to a standing wave phenomenon.

A strong trend from clear to cloudy conditions can be seen during NH summer 1982 in the central and eastern Pacific (160°E–80°W). At about the same time, a trend from relatively cloudy to clear conditions occurs in the western Pacific and Indian Oceans (80°–160°E). These shifts are associated with the onset of the 1982–83 El Niño/Southern Oscillation event (see Rasmusson and Wallace, 1983). The onset of large-scale convection anomalies east of the dateline occurs near the

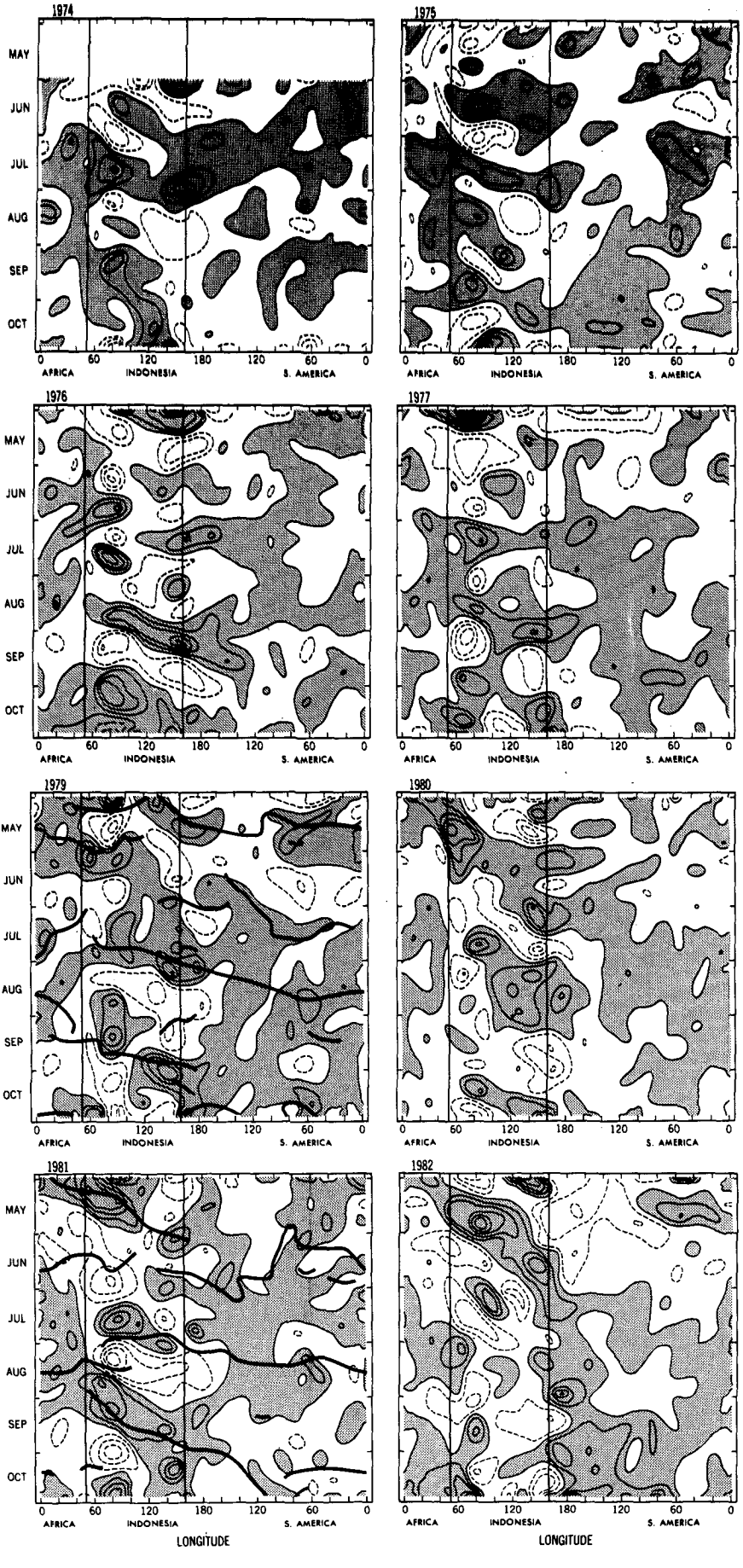
1974
1975
1976
1977
1979
1980
1981
1982
MAY
JUN
JUL
AUG
SEP
OCT
0 60 120 180 120 60 0
AFRICA
INDONESIA
S. AMERICA
LONGITUDE

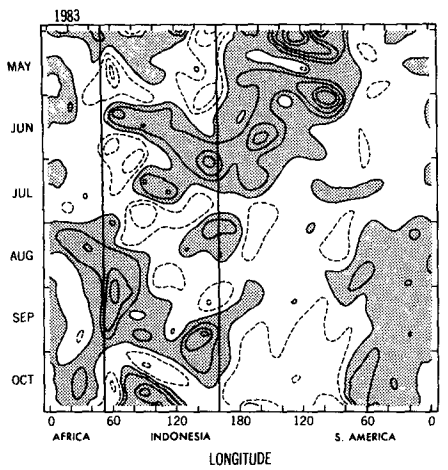

FIG. 4. (*Continued*)

time of arrival of a strong eastward-propagating cloudiness anomaly from the Indian Ocean/western Pacific region. It appears that somewhat weaker intraseasonal oscillations continue after these anomalous conditions are established in the Pacific. The termination of the anomalous conditions is evident around the middle of NH summer 1983.

The OLR Hovmöller diagrams were further analyzed by subjectively fitting straight lines through prominent anomalies in the longitudinal sector 50°–160°E. The time intervals between individual events were estimated by noting the times at which the straight lines intersected the 120°E meridian. The average propagation speeds over the domain (50°–160°E) were estimated from the slopes of the lines. A total of 32 events, or about three to four per six-month period, were identified.

The frequency distribution for the time between events for NH summer (Fig. 5a) shows a broad peak in the 30–60 day range. This method of estimating the oscillation's period is independent of our spectral and cross-spectral analyses, where we selectively examined 28–72 day variations through our choice of Fourier filters. A similar oscillation-period distribution was found by Julian and Madden (1981) based upon 150 mb zonal winds at Truk Island from October 1964 to October 1969. The broad frequency distribution evident in both our results and those of Julian and Madden support our choice of a relatively broad (28–72 day) Fourier filter for the spectral and cross spectral analyses. The frequency distribution of eastward propagation speeds (Fig. 5b) also shows a fair amount of

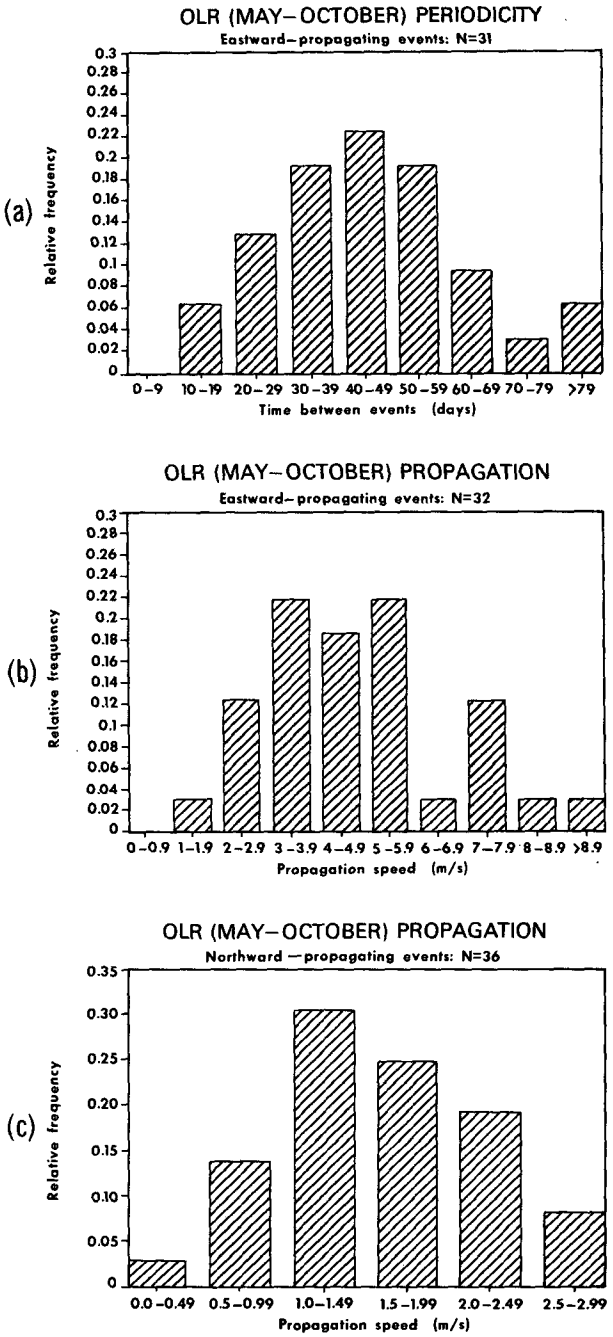

FIG. 5. Frequency distributions for NH summers 1974–83 of observed (a) time intervals between OLR intraseasonal oscillations (31 estimates); (b) average eastward propagation speed of OLR anomalies (32 events); and (c) average northward propagation speeds (36 events) in the Indian monsoon region. Observations were based on subjective line-fit analyses of OLR Hovmöller diagrams. (See text for details.)

FIG. 4. Hovmöller diagrams of intraseasonal OLR anomalies (averaged 5°N–5°S) displayed in longitude vs time format for NH summers 1974–83. Contour interval is 10 W m^{-2}; shading denotes negative OLR (positive convection) anomalies. Vertical lines at 50°E and 160°E denote boundaries of the region analyzed for eastward propagation and periodicity.

variability between events, with typical phase speeds of 3–6 m s^{-1} during NH summer.

A frequency distribution for northward propagation speeds of anomalies in the Indian monsoon region (Fig. 5c) was derived in a similar manner but was based on time–latitude diagrams of OLR anomalies averaged from 60°–90°E and analyzed from 5°S to 25°N (not shown). Figure 5c shows that the most common northward propagation speeds are 1–2 m s^{-1} (36 events). This result is consistent with other estimates of the northward propagation speed based upon winds (Krishnamurti and Subrahmanyam, 1982; T. Murakami et al., 1983) and cloudiness data (Yasunari, 1980).

8. Cross-spectral analysis (U250 vs U250)

A cross-spectral analysis of the 250 mb zonal wind was done using a similar procedure to that used in the OLR analysis (section 6). Analyses were done using 25 centerpoints where the 28–72 day variance exceeded the red noise variance at the 95% significance level. The reference time series were obtained by averaging the center-point time series with the time series of its eight neighboring grid points.

The most noteworthy results for the tropics are for the center point 5°S, 110°W (Fig. 6), in which about 16% of the globe has coherence-squared values significant at the 99% level. The most striking feature is the inferred global-scale eastward propagation in the tropics, where a coherent wavenumber-one structure is present from 20°N–15°S (shaded regions). The unshaded tropical regions generally do not contain significant 28–72 day variability compared to red noise (see Fig. 2d). The global scale wavenumber-one structure of the wind anomalies is consistent with the full-year results of Madden and Julian (1972).

Along individual meridians in the tropics, the wind oscillations are roughly in-phase, although the anomalies at 20°N and 15°S generally lag those near the equator, with the phase difference being up to ¼ cycle. Poleward propagation of upper-air zonal wind anomalies in the tropics is also evident in the results of Murakami et al. (1983; their Fig. 28) and Anderson and Rosen (1983).

The primary extratropical signals in Fig. 6 are zonally elongated bands located in the Southern Hemisphere. Over much of the Pacific and Indian Ocean regions, the anomalies along 30°S are out of phase with the tropical anomalies, while anomalies along 50°S in these regions are roughly in phase with the tropical anomalies. The relative phases along 120°E at 5°, 30° and 55°S illustrate these relationships. The out-of-phase relationship between anomalies along the equator and those along 30°S has been confirmed using Hovmöller diagram analysis. It follows from these phase relationships that the extratropical and tropical anomalies propagate at a similar rate, particularly over the Pacific and eastern Indian Ocean sectors.

In Fig. 2d, there is evidence for significant 28–72 day U250 variability in the North Atlantic. Cross-spectral analyses, using center points in these regions as well as the tropics, do not reveal a significant statistical link between the tropical oscillation and these extratropical fluctuations in the North Atlantic.

The speed of propagation of the tropical U250 anomalies varies with longitude. From 40° to 160°E

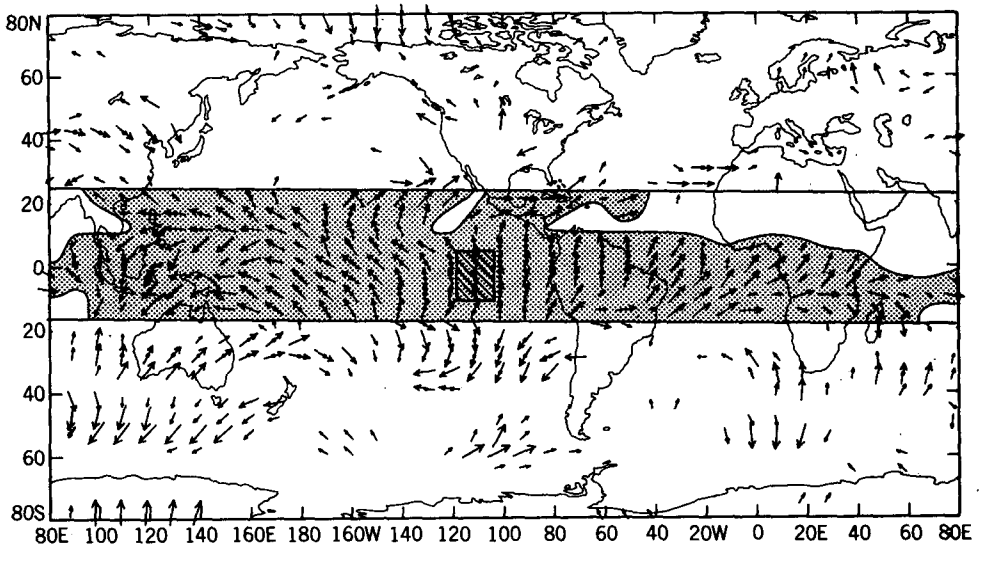

FIG. 6. Phase/coherence map for U250 vs U250 cross spectral analysis, using a nine-point area-averaged reference time series centered at 5°S, 110°W. Arrow lengths are proportional to coherence-squared; directions give the phase of 28–72 day oscillations relative to the reference series. See text and Fig. 3 caption for more details.

the arrows rotate through more than 180° of phase, indicating fairly slow propagation. On the other hand, the arrows rotate more gradually along the tropical strip from 160°E eastward to 40°E, which is the region of fast propagation. Madden and Julian's (1972) cross-spectral analysis results for the 150 mb zonal wind (see their Fig. 8) also indicate a longitudinally varying propagation speed. This phenomenon will be examined further in the later sections.

9. U250 Hovmöller diagram analyses

Based upon Fig. 6, which showed the eastward-propagating tropical U250 anomaly to be present over most of the globe in the band from 0° to 10°S, the wind anomalies were averaged over this latitude band to produce the Hovmöller diagrams in Fig. 7, following the same procedure used for the OLR diagrams in Fig. 4. The added features on the diagrams for 1979 and 1981 will be discussed in section 10.

Inspection reveals that there are large differences between seasons in the prominence of the oscillation. The NH summers 1979, 1980, and 1981 are characterized by strong U250 oscillations. The NH summers 1975–78 show much less evidence for eastward propagation around the globe. At the end of July 1976 and in mid-July 1977 a zonally symmetric pattern appears, with relatively weak positive U250 anomalies nearly continuous around the globe. This apparent trend between the early and later years of the record may be due to a number of effects, including changes in the quality of the wind data, changes in the analysis scheme used by NMC to derive the global circulation, or actual long-term variability in the character of the oscillations. For example, the analysis scheme used to derive the circulation data was changed on 22 September 1978 from the Hough analysis scheme, which produces nearly nondivergent wind fields (Cooley, 1974), to optimum interpolation. Our Hovmöller diagrams show that the character of the U250 oscillations changes significantly at about this time.

The OLR Hovmöller diagrams (Fig. 4) also show some evidence for weaker, slightly higher frequency oscillations in the early years of record, which supports the view that differences are due in part to climatic fluctuations or trends. Anderson et al. (1984) have shown, using a 25-year record of 850 and 200 mb wind data at Truk Island, that the tropical oscillation exhibits a large amount of long-term variability in both amplitude and frequency.

In summary, it is possible that the trend evident in the U250 Hovmöller diagrams is due to a number of factors. In any event, the apparently large interannual variability of the intraseasonal oscillations further illustrates the fact that caution should be used when drawing general inferences about these oscillations based upon data sets of relatively short length.

The strong evidence for eastward propagation of U250 anomalies in our Hovmöller diagrams (particularly for 1979–83) indicates that the wind oscillation is not a dipole phenomenon. The average propagation speed of the tropical U250 anomalies in the "fast" and "slow" regions was estimated using a similar subjective analysis scheme to that of the OLR analysis. For the U250 analysis, a more limited sample was taken using only very prominent oscillations occurring after September 1978. The "fast" region is defined as the longitudinal sector 160°E–0°W, while the "slow" region is defined as the sector 40°–160°E. The average ground speed of the anomalies in the fast region is 15 m s^{-1} for eight occurrences. In the slow region (five occurrences) it is 6 m s^{-1}. Parker (1973) found an average propagation speed of 13–14 m s^{-1} for zonal wind fluctuations in the 70–150 mb region which he identified as Kelvin waves.

10. Relationships between OLR and U250 anomalies

a. Hovmöller diagram analysis

In Fig. 4, features from Hovmöller diagrams for U250 are superimposed on Hovmöller diagrams of OLR for the years 1979 and 1981 to illustrate relationships between the two variables. Northern summers 1979 and 1981 were chosen because they exhibited strong, well-defined oscillations in the U250 Hovmöller diagrams. The solid dark lines in Fig. 4 (1979 and 1981) are taken from the zero contours of the U250 Hovmöller diagrams and show areas where the U250 anomalies are changing from westerly to easterly as time is advancing. Of particular interest are the lines that slope from upper left to lower right in the diagram. These show the approximate location and progression of 250 mb u-component divergence centers associated with eastward-propagating U250 oscillations.[1]

The superimposed features show that in many cases, large convection anomalies are linked to the propagation of the U250 divergence, particularly in the longitude sector 50°–160°E. However, there are some instances of u-component divergence without convection and convection without large-scale divergence. One cannot distinguish from these diagrams whether the divergence is initiating convection or vice versa.

In Fig. 7, negative OLR anomalies from Fig. 4 (averaged 5°N–5°S) have been superimposed on the U250 (averaged 0°–10°S) Hovmöller diagrams for NH summers 1979 and 1981. The hatching shows regions with strong negative OLR anomalies (magnitude of at least 10 W m^2), representing large positive convection anomalies. Both of these diagrams show several cases in which the intensification of wind anomalies during

[1] The u-component divergence referred to in subsequent discussions does not necessarily have the same sign as the divergence of the total wind.

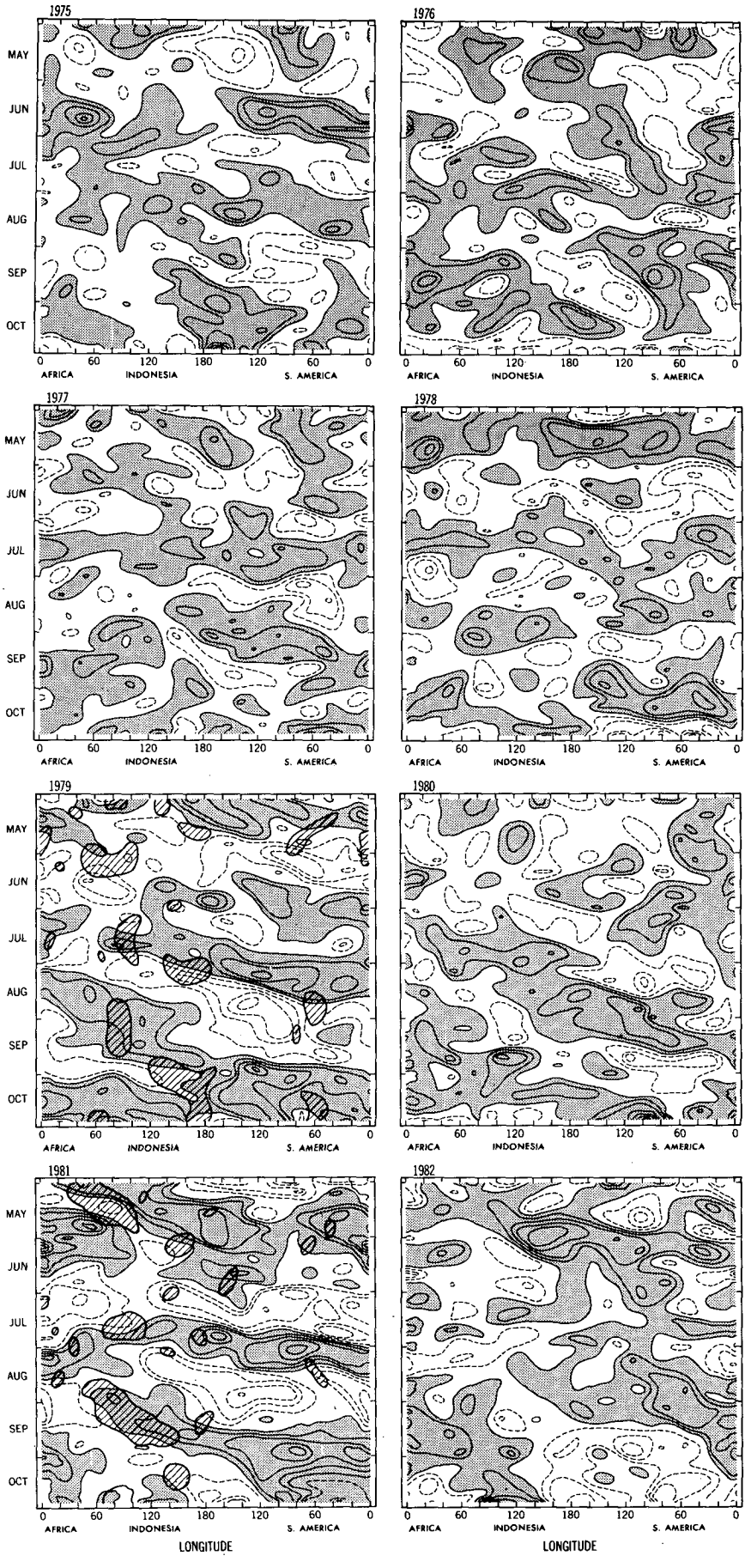
1975
1976
1977
1978
1979
1980
1981
1982
MAY
JUN
JUL
AUG
SEP
OCT
0 60 120 180 120 60 0
AFRICA
INDONESIA
S. AMERICA
LONGITUDE

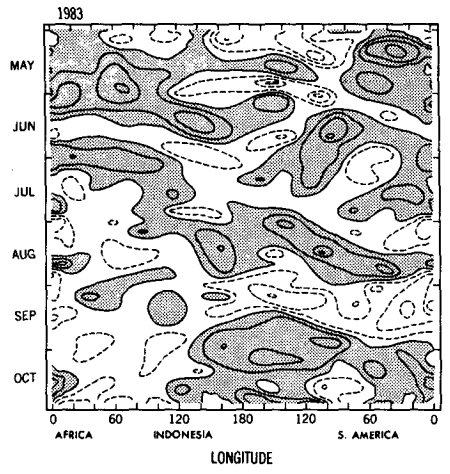

FIG. 7. (*Continued*)

a U250 oscillation is associated with anomalous convection upstream to the west. An example of this occurs in August–September 1981 with a large convection anomaly centered near 90°E preceding the intensification of anomalous westerlies near 160°E in mid-September 1981.

These two diagrams also show instances of strengthening U250 anomalies which do not appear to be related to local anomalies of increased convection. For example, in late September 1981 further strengthening of westerly anomalies occurs near 80°W with no apparent strong convective forcing to the west along 5°N–5°S. This intensification may be related to such factors as tropical convection outside the 5°N–5°S latitude belt, extratropical influences, or even temporal or spatial variations in data quality. A pattern of strengthening U250 anomalies over the central Pacific and reintensification near South America occurs in several of the oscillations.

b. Cross-spectral analysis (OLR vs U250)

Statistically significant relationships between OLR and U250 anomalies are examined using cross-spectral analysis between area-averaged OLR (the reference time series) and a global grid of U250 time series. Eight NH summers are examined, with 1974 and 1978 being excluded because of missing data. The cross-spectral results for the 28–72 day band demonstrate that the features identified in the Hovmöller diagram analyses are statistically significant in an eight-year data set.

Preliminary experiments showed that the area of significant coherence, even at remote locations, was increased when larger areas of in-phase OLR fluctuations were averaged to obtain the reference series. This probably reflects the fact that area averaging reduces the effects of smaller-scale disturbances and emphasizes the larger-scale phenomena. The shaded (in-phase) regions for the four maps in Fig. 3 were used to construct area averaged OLR reference series. The four resulting phase/coherence maps for OLR vs U250 are shown in Fig. 8. The sequence of maps shows the relationship between wind and convection anomalies at approximately 10-day intervals during the oscillation, with the large arrows indicating where peak westerly or easterly 28–72 day U250 anomalies are occurring simultaneously with positive convection (negative OLR) anomalies.

Map A shows that with convection located in the Indian monsoon region and over Indonesia, westerly anomalies are located to the east over the western tropical Pacific. There is relatively little evidence for easterly anomalies upstream to the west and almost no evidence for coherent tropical U250 anomalies over the northern tropical Atlantic, Africa, or the Indian monsoon region. A large region of significant coherence occurs in the tropics over the eastern Pacific, South America and the south Atlantic, where the U250 anomalies are in transition from maximum easterly anomalies to maximum westerly anomalies.

Map B shows that about 10 days later the Pacific convection anomalies have moved north of the equator, while the westerly U250 anomalies in the latitude belt 5°N–15°S appear to be continuing eastward through a region of relatively infrequent convection. These westerly anomalies probably represent the continued eastward progression of the U250 anomalies associated with the equatorial convection shown in map A. In map B, the coherent westerly anomalies south of the equator appear to be more extensive than those in the region directly east of the convection. Thus, while the OLR anomalies during northern summer tend to propagate north from the equator in many regions, the coherent wind anomalies seem to maintain a more prominent structure south of the equator as they progress eastward through the tropics.

Map C shows a continued eastward progression of tropical U250 anomalies, with coherent easterly anomalies over the tropical Pacific and a small region of tropical westerly anomalies in the equatorial Indian Ocean. A large area of coherent fluctuations is found in the Southern Hemisphere, where an interaction may be occurring between atmospheric anomalies in the tropics and those in the Southern Hemisphere extratropics. About 10 days later (map D) the convection has returned to the equatorial Indian ocean, accompanied by anomalous westerlies downstream over In-

FIG. 7. Hovmöller diagrams of intraseasonal U250 anomalies (averaged 0°–10°S) displayed in longitude vs time format for NH summers 1975–83. Shaded regions denote positive U250 (westerly) anomalies. Contour interval is 3 m s^{-1}.

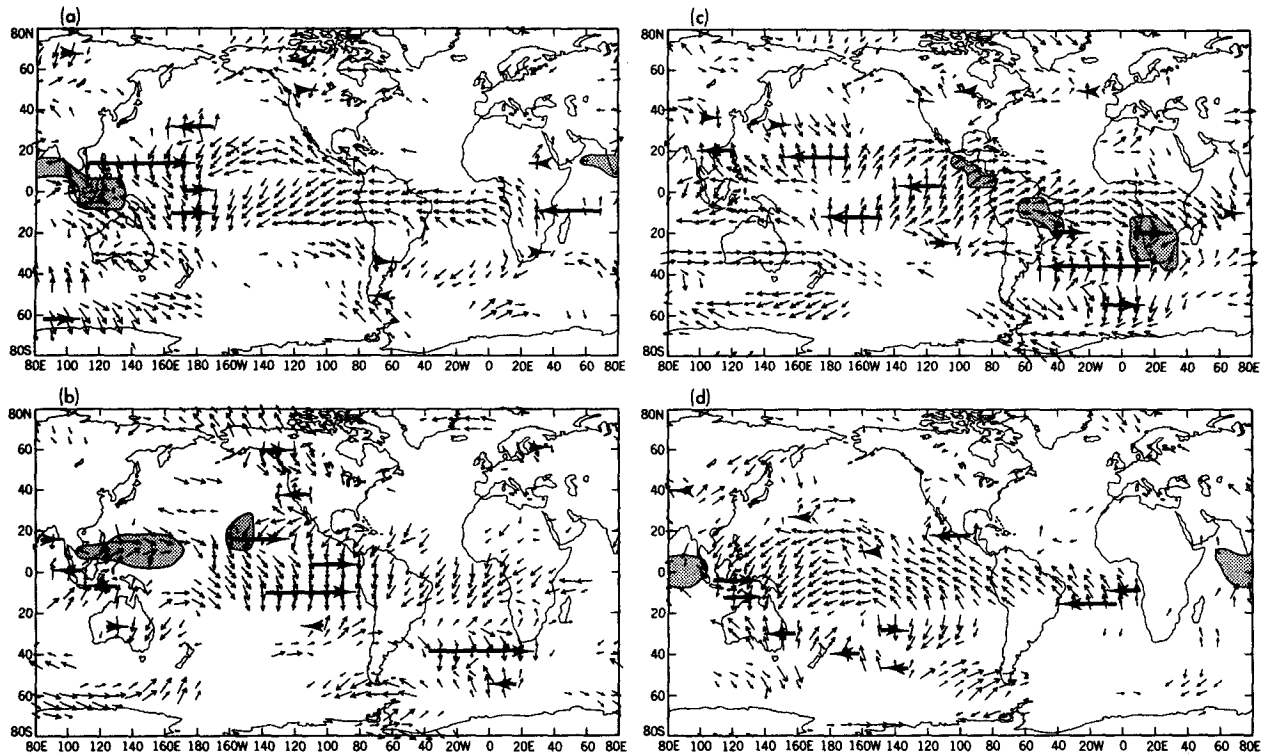

FIG. 8. Phase/coherence maps from 28–72 day cross spectral analysis of OLR vs U250 for eight NH summers. Shaded regions denote the areas averaged to obtain the reference OLR time series and are based on Fig. 3. The four maps represent conditions at time intervals of about ¼ cycle (10 days). Phase and coherence-squared information is given by the direction and length, respectively, of the small arrows (see Fig. 3 caption). Dark arrows are a subjective analysis showing U250 anomaly directions where the U250 anomalies are approximately in-phase or out-of-phase with negative OLR (positive convection) anomalies in the shaded region.

donesia. The easterly anomalies which were located over the tropical Pacific in map C have propagated eastward to the tropical south Atlantic.

A comparison of the four maps in Fig. 8 shows a relatively consistent picture of the relationship between the OLR and U250 anomaly patterns, particularly in the tropics. The areas of significant coherence are roughly the same as for the U250 vs U250 map (Fig. 6), and the phase arrows again indicate an eastward-propagating wavenumber-one signal in the winds. Similar phase relationships as for Fig. 6 exist between the tropical and extratropical U250 anomalies, although map C of Fig. 8 shows a much larger area of significant coherence in the extratropical South Atlantic than does Fig. 6. An important feature is the strong statistical relationship between tropical OLR anomalies and extratropical U250 anomalies in the southern (winter) hemisphere extratropics as compared to the northern (summer) hemisphere extratropics. The phase relationships between the tropical OLR anomalies and U250 anomalies generally indicate 250 mb u-component divergence flanking tropical regions of convection; this result is in agreement with our Hovmöller diagram comparisons.

The tropical results presented here are in general agreement with Madden and Julian's (1972; their Fig. 16) schematic life cycle of a 40–50 day oscillation. Our OLR results in section 6 suggest that significant convection anomalies occur over a somewhat larger portion of the tropics than Madden and Julian indicated, although the most prominent equatorial convection occurs in the areas they noted.

The zonal wind anomalies inferred in Fig. 8 are manifestations of tropical and extratropical circulation features such as strengthened jet streams and anomalous ridge and trough structures. A more detailed description of these features is not attempted here because our analysis results do not show the magnitudes of the zonal wind anomalies or the nature of the meridional wind anomalies.

11. Discussion

a. Introduction

The primary result of this study is the identification and description of a global-scale 30–60 day tropical oscillation of OLR (cloudiness) and 250 mb zonal winds during the northern summer. Both the OLR and U250 fluctuations show evidence for eastward propagation and a zonal wavenumber-one structure. The U250 anomalies have a more consistent global-scale structure and propagation characteristics while the OLR anomalies are most prominent in the Indian Ocean and western tropical Pacific. The OLR anom-

alies also exhibit prominent northward propagation from the equator in the NH summer monsoon region. In most cases, the tropical 250 mb u-component anomalies are dynamically consistent with the OLR anomalies, showing anomalous upper-air u-component divergence flanking regions of convection.

While many interesting features of the intraseasonal tropical oscillation have been documented in this and other studies, many important questions remain unanswered. Perhaps the two most important theoretical questions are the following:

1) Why does the oscillation have a 30–60 day time scale?
2) What causes the observed propagation of OLR and U250 anomalies?

Several theories of the tropical oscillation have been offered to explain the observed time scale and the nature of the interaction between the circulation and convection during the oscillation. These theories are not fully examined here because we have not examined other atmospheric variables such as meridional winds, moisture, and temperature, which also play important roles. In the context of the observations discussed in this paper, the theories are divided into two major viewpoints.

In the first group of theories—the equatorial wave viewpoint—the time scale is controlled by the time for a circulation feature to propagate around the globe in the tropics. This hypothesis was suggested by Madden and Julian (1972) who found that a tropopause height perturbation propagated around the globe once per oscillation. Chang (1977) suggested that eastward-propagating equatorial Kelvin waves were responsible for the time scale.

Presumably, in theories of this type the upper-air divergence associated with a traveling wave propagates into a region, triggering increased convective activity. The convection in turn acts to strengthen the upper-air divergence associated with the wave. The observed propagation of convection is controlled by the progression of the wind anomalies, although the particular spatial response of the convection depends on boundary conditions such as sea surface temperatures, lapse rates, and moisture availability.

A major problem with an equatorial Kelvin wave theory of the oscillation is that the observed propagation speed of the wind anomalies (10–15 m s^{-1}) is much less than the phase speed predicted by theory for a warm-core baroclinic Kelvin wave (30–50 m s^{-1} according to Lim and Chang, 1983). Chang (1977) has suggested that the vertical mixing of vorticity and momentum in convective regions justifies the inclusion of a cumulus friction term in the shallow water equations. He showed that the cumulus damping term could produce theoretical phase speeds in closer agreement with the observations. (See, also, the comments of Stevens and White, 1979.) A second major problem with the Kelvin wave theory is that, according to Murakami et al. (1983), the phase relationships between zonal winds and geopotential heights during the oscillation do not resemble those of a Kelvin wave. It is evident that further work must be done to establish a more detailed view of the oscillation's structure.

In the second group of theories—the convective forcing viewpoint—the oscillation derives its fundamental time scale from some process other than a wave traveling around the globe. The convection acts as a forcing for observed eastward-propagating circulation features. Yamagata and Hayashi (1984) have recently examined the response of the forced shallow water equations to a specified localized oscillatory heating with a 40-day period. Proposed mechanisms which might determine the convection's time scale include cloudiness/albedo effects (Sikka and Gadgil, 1980), surface hydrological processes (Webster, 1983), extratropical influences (Yasunari, 1981), or processes associated with the Hadley circulation (Anderson, 1984; Goswami and Shukla, 1984).

For example, Anderson (1984) identified a class of slowly oscillating circulation modes in a model of the tropical atmosphere which included a Hadley cell basic state. The 40–50 day time scale of these modes results from the advection of perturbation quantities by the basic state Hadley circulation; Anderson proposed that the modes affected tropical convection by modulating the atmospheric static stability.

b. Interpretation of results

Our observational study has revealed several characteristics of the oscillation for the NH summer season which will be interpreted and discussed in the context of the theoretical viewpoints discussed previously.

1) The eastward-propagating U250 anomaly is of global extent, circling the globe once per 30–60 days. The U250 vs U250 cross-spectral analysis (Fig. 6) shows that on average the zonal wind anomalies travel around the globe once per 30–60 days while the Hovmöller diagrams show that this feature is most prominent after 1978. However, the Hovmöller diagrams (Fig. 7) also show that the prominent eastward-propagating anomalies after 1978 often have gaps in their banded structure. For example, the large westerly anomalies in mid-July 1981 do not appear to be a result of continued eastward progression of the large westerly anomalies which occurred during May and June. The organized global-scale structure lends support to the equatorial wave viewpoint, although the gaps in the structures suggest that the features may be a response to a forcing rather than an initiator of convection.

An interesting theoretical question concerns how the observed circulation anomalies are maintained against frictional dissipation as they propagate around the globe on a time scale of 30 to 60 days. A possibility suggested by our OLR analysis is that convective forcing occurring in various parts of the tropics counteracts some of the frictional effects.

2) The average ground speed of the U250 anomalies varies with longitude from an observed ground speed of 6 m s^{-1} in the "slow" region (40°–160°E) to a speed of 15 m s^{-1} in the "fast" region (160°E–0°W). If one adopts the viewpoint that the U250 anomalies are a propagating wave, then these longitudinal changes in the wave ground speed can result from changes in the basic state through which a wave of constant phase speed is traveling, or from changes in the actual phase speed of the wave. In equation form, $c_0(x) = U(x) + c_n(x)$, so that changes in observed ground speed, $c_0(x)$, can result from local Doppler-shifting by the time-mean basic state, $U(x)$, or from changes in the wave's "natural" phase speed, $c_n(x)$, where x denotes the zonal direction. We define the "natural" phase speed as the speed of the wave in the absence of base state flow and in the absence of zonally varying base state parameters (e.g., static stability or damping).

The first possibility can be examined by calculating the seasonal mean basic states for the fast and slow regions. These values were found for the 250 mb zonal wind alone and for a "vertically averaged" zonal wind which was approximated by the average of the 850 and 250 mb u-components. The results are summarized in Table 1. The estimated natural phase speeds in the fast region are 2–7 m s^{-1} larger than the estimated phase speeds in the slow region, depending on the basic state used. Given the crudeness of these estimates, the results must be considered tentative, but they indicate that the propagating U250 anomalies might be interpreted as a wave of constant phase speed relative to the *250 mb* zonal wind basic state.

Anderson et al. (1984) also addressed the question of the phase speed of the oscillation by analyzing the seasonality of the oscillation's period. Assuming that the propagation speed of the wave is constant relative to the base state, they noted that the oscillation's period should vary from 66 days to 36 days due to the annual cycle of the base state. Their examination of a 25-year data set of zonal wind shear over Truk Island revealed no statistically significant seasonal variation of periodicity.

The second possibility is that longitudinal changes in the "natural" phase speed of the wave may contribute to changes in the observed ground speed. The reasons for such changes in the phase speed may be complex. One possibility suggested by our cross-spectral results is that the intensity and latitudinal location of the anomalous convective forcing changes between the fast and slow regions. For example, the convection occurs further from the equator in the fast region, which implies that it is no longer an efficient forcing mechanism for equatorial Kelvin waves (Gill, 1980). The convection is more intense in the slow region, which means that the cumulus friction mechanisms described by Chang (1977) might be partly responsible for the slower phase speeds. It is evident that further theoretical or modeling studies are needed to determine the precise cause of the eastward propagation of the circulation features observed in this study.

3) Prominent northward propagation of OLR anomalies occurs in the Indian monsoon region as break monsoon conditions are replaced by active monsoon conditions. The northward propagating OLR anomalies are phase-locked with eastward propagating OLR anomalies since they occur simultaneously along the equator south of India.

If one adopts the equatorial wave viewpoint, convective activity along the equator is initiated by an eastward-propagating equatorial wave after which the convection migrates northward into the Indian monsoon region. From this viewpoint, the active/break cycle in the monsoon is a remote response to quasi-periodic wind anomalies in the equatorial belt. Alternatively, if one adopts the convective forcing viewpoint, the active-break cycle in the monsoon derives its characteristic time scale from other processes and acts as a quasi-periodic forcing for the tropical circulation features noted in this study. In any case, the development of a convection region near the equator and its subsequent northward migration into the monsoon region is a prominent NH summer feature which any realistic model of the oscillation should be able to reproduce.

Webster (1983) has shown that the northward propagation and low-frequency variability of monsoon convection can be simulated when a full hydrological cycle is included in a zonally symmetric land–ocean model. The important mechanisms he identified in-

TABLE 1. Analysis of U250 anomaly phase speed.

Longitude domain	Observed* ground speed c_0 (m s^{-1})	Zonal wind† basic state U (m s^{-1})	Natural# phase speed c_n (m s^{-1})
Fast region (160°E–0°W)	14.7	+1.6 (250 mb)	13.1
	14.7	−2.1 (850 and 250 mb)	16.8
Slow region (40°–160°E)	6.4	−4.3 (250 mb)	10.7
	6.4	−3.5 (850 and 250 mb)	9.6

* Average ground speed for longitude domain; based on eight occurrences (fast region) and five occurrences (slow region) of the oscillation after September 1978.

† Calculated for latitudinal domain 0°–10°S; average of nine NH summer seasons.

Calculated as $c_n = c_0 - U$.

clude large sensible heat flux in the dry, clear area ahead (north) of the convection and evaporative cooling over the moist ground behind the propagating convection. These effects modulate the total heating, which in turn modulates the vertical motion in the model.

4) Coherent OLR anomalies, characterized by wavenumber-one zonal structure, are scattered throughout the tropics, although the most prominent anomalies are found in the Indian Ocean and western Pacific. The OLR anomalies are consistent in phase with the u-component divergence associated with the wavenumber-one U250 anomaly. However, the Hovmöller diagrams (Fig. 4) and the OLR 28–72 day variance map (Fig. 1c) show that the wavenumber-one zonal structure is asymmetric in amplitude, with the largest OLR variations occurring as a dipole-like fluctuation (linked by eastward-propagating features) in the Indian Ocean and western Pacific. The magnitude and dynamical importance of convection fluctuations in the remainder of the tropics is not known, although the organized large-scale structure of the OLR anomalies may be an important feature of the oscillation. The eastward-progressing convection anomalies, which have a markedly different speed from the northward propagating anomalies in the Indian monsoon region, appear to be a consistent and important feature of the oscillation.

5) U250 fluctuations in the *Northern* Hemisphere tropics over the Atlantic, Africa, and the Indian monsoon region (unshaded tropical regions, Fig. 6) do not exhibit significant coherence at 28–72 days with the major oscillation in OLR/U250 over the remainder of the tropics. The OLR vs U250 cross-spectral results (Fig. 8) also show a lack of prominent areas of coherent U250 fluctuations over these regions. This is a surprising result since one might expect large variations in the tropical easterly jet to occur as the monsoon convection fluctuates (Krishnamurti and Bhalme, 1976). However, according to Koteswaram (1958), the strongest winds in the tropical easterly jet are found near 100–150 mb which suggests that by using only the 250 mb level to study winds in the Indian monsoon region, our ability to accurately monitor changes in the tropical easterly jet may be limited.

The lack of a coherent zonal-wind fluctuation at 250 mb over parts of the globe may also be due to other factors, such as longitudinal variations in the base state. One possibility is that the U250 anomaly is a wave phenomenon which cannot propagate into regions where the easterly base state winds exceed some critical value, such as the westerly phase speed of the wave. The NH summer-mean U250 map (Fig. 2a) shows that in the tropical strip, most of the regions that have low coherence in Fig. 6 also have mean easterly winds at 250 mb. However, Figs. 2a and 6 also show that near Indonesia, significant coherence is found in a region of fairly strong mean easterlies at 250 mb.

Our Hovmöller diagram analysis indicates that a maximum intensification of westerly U250 anomalies along 0°–10°S occurs to the east of major convection anomalies. In a similar manner, the maximum 250 mb zonal wind anomalies associated with the Indian monsoon region convection may be occurring east of the monsoon region.

Our discussion thus far has focused on the question of whether wavenumber one circulation anomalies modulate the tropical convection or whether convection anomalies force a wavenumber one response in the circulation. In attempts to explain the global-scale eastward progression of the anomalies, few theories have dealt with the *interaction* of convection and circulation anomalies. Stevens and Lindzen (1978) have suggested that the tropical wave-CISK mechanism may be involved in the oscillation. A possibility suggested by the results of our study is that the eastward movement results from an eastward propagating circulation feature which triggers convection in regions where conditions are favorable for convective activity. Rather than propagating around the entire globe as a free wave, the circulation anomalies may initiate new convection before dissipating as they progress eastward from the original convective region. The new convection could produce more wind anomalies—which may resemble the theoretical equatorial Kelvin wave or Rossby wave solutions described by Gill (1980) or Lim and Chang (1983)—which could cause the anomalies to continue their eastward progression.

From this viewpoint, the propagation speed of the anomaly might not be expected to agree with the constant phase speed predicted by theory for a free equatorial Kelvin wave. The ground propagation speed may depend on several factors, such as the strength and persistence of convection in various regions and the zonal wind basic state.

12. Conclusions and suggestions for future work

Based upon intraseasonal Hovmöller diagrams and 28–72 day cross-spectral analysis of OLR and U250, we have described features of a tropical intraseasonal circulation-convection oscillation having a typical time scale of 30–60 days. While many previous studies have examined the oscillation's behavior during a single season, our results are based on more than 30 events occurring in NH summers 1974–83.

Both OLR and U250 oscillations exhibit characteristics of a zonal wavenumber-one structure although this feature is most evident for the U250 anomalies. The U250 anomalies propagate at about 6 m s^{-1} near the region of strong 30–60 day equatorial convection oscillations (40°–160°E), while they propagate at about 15 m s^{-1} from 160°E–0°W. These changes in zonal propagation speed may be due largely to longitudinal changes in the basic state of the zonal wind, although other factors (suchs as differences in the convection) may be involved as well.

Prominent northward propagation (at 1–2 m s^{-1}) of OLR anomalies occurs in the Indian monsoon region.

Convection anomalies also propagate eastward (at 3–6 m s^{-1}) along the equator from 50° to 160°E before moving north of the equator in the western tropical Pacific. The eastward- and northward-propagating OLR anomalies are phase-locked, since they occur simultaneously along the equator south of India. Centers of maximum (out-of-phase) 28–72 day OLR variability in the Indian Ocean and western tropical Pacific appear to be associated with these propagating features.

Analysis of Hovmöller diagrams (Figs. 4 and 7) shows that the eastward-propagating OLR anomalies in the Indian Ocean and Western Pacific are related to eastward-propagating U250 divergence anomalies. Cross-spectral analysis of OLR vs U250 (28–72 day spectral band) indicates that convection anomalies throughout the tropics are flanked by anomalous 250 mb *u*-component divergence. While the eastward-propagating U250 divergence anomalies may indicate a dynamical link between convection occurring in remote regions of the tropics, it is also possible that the U250 anomalies are a response to a convective forcing that is initiated by other processes.

The question of the forcing vs response roles of the convection and circulation is a difficult one because of the strong interaction between the processes. The observations show that the circulation and convection anomalies have an organized structure and systematic time evolution. Some evidence has been presented that equatorial waves may play an important role in the oscillation although the most fundamental questions about the oscillation's time scale and propagation characteristics remain unanswered.

It is apparent that further observational and theoretical studies are necessary to answer basic questions about the oscillation. Future observational studies should be undertaken to determine the role of other atmospheric variables, such as low-level winds, moisture, surface heating, lapse rates, etc. Because the oscillation exhibits considerable variability between events, the combined use of composites and individual case studies is recommended.

Modeling efforts often attempt to find the simplest possible scheme that still retains the basic features of a phenomenon. Our study suggests that longitudinal variations in the model base state may be needed to achieve a realistic simulation of the intraseasonal oscillation. For example, the convection signal is scattered throughout the tropics but is generally not found in areas with low sea surface temperatures; coherent U250 anomalies are generally found away from strong easterly 250 mb base flow. Furthermore, our results suggest that a realistic model of the oscillation may need to include interaction between convection and circulation terms, with circulation anomalies modulating the convective forcing and vice versa.

Another important theoretical question that merits further study concerns the interaction between tropical and extratropical convection and wind anomalies during an oscillation. We have shown that 250 mb zonal wind anomalies in the Southern Hemisphere extratropics are strongly coherent with OLR and U250 anomalies in the tropics during NH summer.

An important test of any theory of the oscillation is its ability to reproduce the observed characteristics *throughout the seasonal cycle* as documented by this report and WLK. In a forthcoming paper, we will examine the seasonality of the oscillation in relation to the large seasonal changes in the base state of the winds and convection. Future study of the intraseasonal oscillation in relation to seasonal and interannual variations should bring further progress in understanding its origin and life cycle.

Acknowledgments. This research was supported by NOAA Grant NA-79AA-D-00129 and NSF Grant ATM82-19079. Jeffrey Varanyak did much of the graphics work.

REFERENCES

Anderson, J. R., 1984: Slow motions in the tropical troposphere. PhD. thesis, Colorado State University, Atmos. Sci. Paper No. 381, 144 pp.

——, and R. D. Rosen, 1983: The latitude height structure of 40–50 day variations in atmospheric angular momentum. *J. Atmos. Sci.*, **40**, 1584–1591.

——, D. E. Stevens and P. R. Julian, 1984: Temporal variations of the tropical 40–50 day oscillation. *Mon. Wea. Rev.*, **112**, 2431–2438.

Bergman, K. H., 1979: Multivariate analysis of temperatures and winds using optimum interpolation. *Mon. Wea. Rev.*, **107**, 1423–1444.

Chang, C.-P., 1977: Viscous internal gravity waves and low-frequency oscillations in the tropics. *J. Atmos. Sci.*, **34**, 901–910.

Cooley, D. S., 1974: A description of the Flattery global analysis method, no. 1. Tech. Proc. Bull. No. 105. NWS, NOAA, 9 pp.

Flattery, T., 1971: Spectral models for global analysis and forecasting. *Proc. Sixth AWS Technical Exchange Conf.*, U.S. Naval Academy, Annapolis, Air Weather Service Tech. Rep. 242, 42–54.

Gill, A. E., 1980: Some simple solutions for heat-induced tropical circulation. *Quart. J. Roy. Meteor. Soc.*, **106**, 447–462.

Gilman, D. L., F. J. Fuglister and J. M. Mitchell, Jr., 1963: On the power spectrum of red noise. *J. Atmos. Sci.*, **20**, 182–184.

Goswami, B. N., and J. Shukla, 1984: Quasi-periodic oscillations in a symmetric general circulation model. *J. Atmos. Sci.*, **41**, 20–37.

Gruber, A., and J. S. Winston, 1978: Earth-atmosphere radiative heating based on NOAA scanning radiometer measurements. *Bull. Amer. Meteor. Soc.*, **59**, 1570–1573.

Julian, P. R., 1975: Comments on the determination of significance levels of the coherence statistic. *J. Atmos. Sci.*, **32**, 836–837.

——, and R. A. Madden, 1981: Comments on a paper by T. Yasunari, A quasi-stationary appearance of 30 to 40 day period in the cloudiness fluctuations during the summer monsoon over India. *J. Meteor. Soc. Japan*, **59**, 435–437.

Koteswaram, P., 1958: The easterly jet stream in the tropics. *Tellus*, **10**, 43–57.

Krishnamurti, T. N., and H. N. Bhalme, 1976: Oscillations of a monsoon system. Part I: Observational aspects. *J. Atmos. Sci.*, **33**, 1937–1954.

——, and D. Subrahmanyam, 1982: The 30–50 day mode at 850 mb during MONEX. *J. Atmos. Sci.*, **39**, 2088–2095.

——, P. K. Jayakumar, J. Sheng, N. Surgi and A. Kumar, 1985: Divergent circulations on the 30 to 50 day time scale. *J. Atmos. Sci.*, **42**, 364–375.

Kutzbach, J. E., and K. M. Weickmann, 1984: The global distribution of the annual and semi-annual cycles of outgoing long-wave radiation and 250 mb *u*-component winds. *Studies in Climate,* H. van Loon, Ed., Tech. Note NCAR/TN-227+STR, 44–64.

Lau, K. M., and P. H. Chan, 1983a: Short-term climate variability and atmospheric teleconnections from satellite-observed outgoing longwave radiation. Part I: Simultaneous relationships. *J. Atmos. Sci.,* **40,** 2735–2750.

——, and ——, 1983b: Short-term climate variability and atmospheric teleconnections from satellite-observed outgoing longwave radiation. Part II: Lagged correlations. *J. Atmos. Sci.,* **40,** 2751–2767.

Lim, H., and C.-P. Chang, 1983: Dynamics of teleconnections and Walker circulations forced by equatorial heating. *J. Atmos. Sci.,* **40,** 1897–1915.

Lorenc, A. C., 1984: The evolution of planetary-scale 200 mb divergent flow during the FGGE year. *Quart. J. Roy. Meteor. Soc.,* **110,** 427–441.

Madden, R. A., and P. R. Julian, 1971: Detection of a 40–50 day oscillation in the zonal wind in the tropical Pacific. *J. Atmos. Sci.,* **28,** 702–708.

——, and ——, 1972: Description of global-scale circulation cells in the tropics with a 40–50 day period. *J. Atmos. Sci.,* **29,** 1109–1123.

Maruyama, T., 1982: Upper tropospheric zonal wind oscillation with a 30–50 day period over the equatorial western Pacific observed in cloud movement vectors. *J. Meteor. Soc. Japan,* **60,** 172–181.

McPherson, R. D., K. H. Bergman, R. E. Kistler, G. E. Rasch and D. S. Gordon, 1979: The NMC operational global data assimilation system. *Mon. Wea. Rev.,* **107,** 1445–1461.

Murakami, M., 1984: Analysis of deep convective activity over the western Pacific and southeast Asia. Part II: Seasonal and intraseasonal variations during northern summer. *J. Meteor. Soc. Japan,* **62,** 88–108.

Murakami, T., T. Nakazawa and J. He, 1983: *40–50 Day Oscillations During the 1979 Northern Hemisphere Summer.* University of Hawaii (UHMET 83-02), 133 pp.

Parker, D. E., 1973: Equatorial Kelvin waves at 100 millibars. *Quart. J. Roy. Meteor. Soc.,* **99,** 116–129.

Quah, L.-C., 1984: On the 30–50 day oscillation during the 1978–79 northern winter. *J. Meteor. Soc. Japan,* **62,** 261–272.

Rasmusson, E. M., and J. M. Wallace, 1983: Meteorological aspects of the El Niño/Southern Oscillation. *Science,* **222,** 1195–1202.

Rayner, J. N., 1971: *An Introduction to Spectral Analysis.* Pion Ltd., 174 pp.

Sikka, D. R., and S. Gadgil, 1980: On the maximum cloud zone and the ITCZ over Indian longitudes during the Southwest monsoon. *Mon. Wea. Rev.,* **108,** 1840–1853.

Stevens, D. E., and R. S. Lindzen, 1978: Tropical wave-CISK with a moisture budget and cumulus friction. *J. Atmos. Sci.,* **35,** 940–961.

——, and G. H. White, 1979: Comments on "Viscous internal gravity waves and low-frequency oscillations in the tropics." *J. Atmos. Sci.,* **36,** 545–546.

Takeda, T., and M. Ikeyama, 1984: Time variation of cloud amount with about 30-days period in the western North Pacific region. *J. Meteor. Soc. Japan,* **62,** 165–171.

Webster, P. J., 1983: Mechanisms of monsoon low-frequency variability: Surface hydrological effects. *J. Atmos. Sci.,* **40,** 2110–2124.

Weickmann, K. M., 1983: Intraseasonal circulation and outgoing longwave radiation modes during Northern Hemisphere winter. *Mon. Wea. Rev.,* **111,** 1838–1858.

——, G. R. Lussky and J. E. Kutzbach, 1985: Intraseasonal (30–60 day) fluctuations of outgoing longwave radiation and 250 mb streamfunction during northern winter. *Mon. Wea. Rev.,* **113,** 941–961.

Yamagata, T., and Y. Hayashi, 1984: A simple diagnostic model for the 30–50 day oscillation in the tropics. *J. Meteor. Soc. Japan,* **62,** 709–717.

Yasunari, T., 1980: A quasi-stationary appearance of 30 to 40 day period in the cloudiness fluctuations during the summer monsoon over India. *J. Meteor. Soc. Japan,* **58,** 225–229.

——, 1981: Structure of an Indian summer monsoon system with a period around 40 days. *J. Meteor. Soc. Japan,* **59,** 336–354.